Indian Journal of Chemical Technology
Vol. 33, January 2026, pp. 11-19
DOI: 10.56042/ijct.v33i1.22701

Deep eutectic solvent-mediated synthesis of W-Mo oxide nanocomposites for enhanced and tunable photochromic response

A. A. Ajayi[1,2]*, O. Oderinde[3]*, S. O Ogunbayo[1], O.O Ayoni[4], R. A Olawuyi[1] & A. O. Agbeja[1,5]

[1]Department of Chemistry, Faculty of Natural and Applied Sciences, Lead City University, Ibadan, Nigeria

[2]Department of Science Laboratory Technology, School of Pure and Applied Sciences, Federal Polytechnic Ilaro, PMB 50, Ilaro, Nigeria

[3]Department of Chemistry, Nile University of Nigeria, Plot 681, Cadastral Zone C, Research & Institution Area, Airport Road, Jabi Abuja 900108 Nigeria

[4]Department of Chemical Sciences, Faculty of Sciences, Taraba State University, PMB 1167, Jalingo, Nigeria

[5]Department of Sustainable Forest Management, Forestry Research Institute of Nigeria, PMB 5054, Ibadan, Nigeria

*E-mail: adetola.ajayi@federalpolyilaro.edu.ng(AAA) / yinkaoderinde@yahoo.com(OO)

Received 13 August 2025; accepted 14 November 2025

This study details the synthesis and characterization of photochromic tungsten-molybdenum oxide (W-Mo) nanocomposites using a deep eutectic solvent (Ethaline) composed of choline chloride and ethylene glycol in a 1:2 molar ratio, providing a green and efficient fabrication route. FTIR analysis confirmed the successful incorporation of metal oxides into the DES matrix, evidenced by characteristic metal-oxygen (W-O and Mo-O) stretching vibrations observed within the 947-767 cm^{-1} and functional group interactions. Scanning electron microscopy imaging revealed agglomerated, irregularly shaped particles with porous morphologies, while energy dispersive X-ray spectroscopy confirmed the homogeneous distribution of W and Mo within the composite. X-Ray diffraction patterns indicated a predominantly amorphous structure with broad peaks corresponding to semicrystalline tungsten and molybdenum oxide phases. Ultraviolet-visible spectroscopy showed strong absorption in the 259-476 nm range, confirming efficient light-induced activation. The nanocomposites exhibited excellent photochromic performance, transitioning rapidly from cream-yellow to blue within three seconds under UV exposure, and reversibly fading in an oxygen-rich environment within 50 min. Electrochemical impedance spectroscopy (EIS) further revealed that the W-Mo (0.8:0.2) composite had the lowest charge transfer resistance, enhancing electron transport and accelerating photo-switching behaviour. The combined structural, optical, and electrochemical properties of these materials underscore their promise for use in smart windows, UV sensors, and dynamic display technologies.

Keywords: Deep eutectic solvent, Molybdenum oxide, Photochromism, Tungsten oxide

Introduction

Photochromism is a reversible optical phenomenon in which a material undergoes a distinct colour change when exposed to light, transitioning between two states with different absorption spectra[1,2]. This unique property has attracted considerable attention for applications in ophthalmic lenses, smart windows, optical data storage, and various optoelectronic devices[3]. While early research in photochromic systems primarily focused on organic compounds due to their tunable properties, recent advancements have shifted towards inorganic materials[4]. Inorganic photochromic systems are now favoured due to their superior thermal stability, mechanical robustness, chemical resistance, and long-term durability under repeated cycling. Among inorganic systems, transition metal oxides (TMOs) have emerged as promising candidates owing to their adjustable electronic structures, broad-spectrum light responsiveness, and structural versatility[5]. These oxides, particularly tungsten oxide (WO_3), molybdenum oxide (MoO_3), titanium dioxide (TiO_2), and vanadium pentoxide (V_2O_5) are capable of undergoing redox-driven photochromic transformations involving changes in metal oxidation states and ion intercalation[6]. Transition metal oxides are also advantageous for their low toxicity, strong visible and near-infrared light responsiveness, and potential for integration into thin films, coatings, and nanostructured devices[7].

Tungsten oxide (WO_3) is notable among TMOs due to its well-established photochromic and electrochromic properties[8]. Its coloration mechanism usually involveslight-induced electron transfer that reduces W^{6+} to W^{5+} or W^{4+}, accompanied by H^+ ion intercalation into the lattice, forming tungsten bronzes (H_xWO_3). This process produces a visible colour change from pale

yellow or transparent to intense blue[9]. However, traditional WO_3-based photochromic systems face challenges like slow response times, limited reversibility, and narrow spectral operation windows[10]. To address these issues, recent strategies have focused on nano-structuring into nanosheets, nanorods, and hierarchical architectures and doping with other transition metals such as cerium (Ce) and copper (Cu)[11]. These modifications can adjust the bandgap, create oxygen vacancies, and enhance charge transport, thereby improving both coloration efficiency and recovery speed[12]. For example, Cu-doping causes lattice distortions and electronic defects that enable faster electron movement, while Ti-doping boosts visible-light sensitivity and active site availability[13]. Another effective approach is fabricating heterojunctions between WO_3 and other TMOs or semiconductors such as ZnO, Fe_2O_3, or V_2O_5. These hybrid systems benefit from interfacial charge separation, broader light absorption, and increased cycling stability, making them more suitable for real-world applications. The synergy between different oxides in these heterostructures enhances light-matter interaction and improves photo-induced charge transferefficiency[14]. The synthesis of these functional oxide nanocomposites can be done through various techniques, each offering specific advantages in controlling morphology, crystallinity, and composition. Common methods include sol-gel processing, hydrothermal and solvothermal methods, co-precipitation, electrospinning and spray pyrolysis, thermal decomposition and combustion, and microwave-assisted synthesis[15].

In recent years, the use of deep eutectic solvents (DESs) has gained attention as a sustainable, non-toxic, and multifunctional alternative[16]. Deep eutectic solvents, formed through hydrogen bond interactions between donor and acceptor components, exhibit a much lower melting point than their individual constituents. They not only serve as reaction media but also act as templating or structure-directing agents, offering control over particle size, porosity, and morphology[17]. However, this study reports the DES-assisted synthesis of a binary transition metal oxide nanocomposite, incorporating WO_3 and MoO_3, with outstanding photochromic performance.

Experimental Section

Materials

Analytical-grade chemical reagents used to synthesize the materials include glacial acetic acid (CH_3COOH, 99.5%) and ethylene glycol ($C_2H_6O_2$, 99.0%), both purchased from Dow Chemical, USA. Choline chloride ($C_5H_{14}ClNO$, 98.0%) was obtained from Eastman Chemical Co. Ltd, USA while sodium molybdate tetrahydrate ($Na_2MoO_4 \cdot 4H_2O$, 99.0%) was supplied by Sinopharm Chemical Reagent Co. Ltd, China. In addition, absolute ethanol (C_2H_5OH, 99.8%) and sodium tungstate (Na_2WO_4, 98.5%) were procured from Shanghai Yuanye BioTech Co. Ltd, China. Another batch of absolute ethanol was sourced from Mitsubishi Chemical, Japan.

DES Preparation

The deep eutectic solvent (ethaline) was synthesized by combining choline chloride and ethylene glycol in a molar ratio of 1:2. The mixture was stirred vigorously at 80°C for 45 min until a clear and homogeneous solution was obtained, following the procedure outlined in prior studies[19]. This solution was then maintained under vacuum at the same temperature to ensure stability before being used to prepare the WO_3-MoO_3 composite.

Synthesis of Mo-doped WO_3 nanocomposite

The W-Mo(E) nanocomposite was prepared by dissolving sodium tungstate (WO_3, 0.9 g) and sodium molybdate (MoO_3, 0.1 g) in 10 mL of an ethaline (DES). The solution was stirred magnetically at 60°C for 45 min to ensure complete dissolution and uniform dispersion of the precursors. Thereafter, 5 mL of glacial acetic acid was introduced to the solution to reduce the pH and facilitate the formation of coordination complexes. Thereafter, the mixture was further stirred for another 120 min to allow the reaction to proceed to completion. The resulting product, labelled W-Mo(E) 0.9:0.1, was separated by centrifugation, rinsed several times with absolute ethanol to remove residual impurities, and then dried in a conventional oven at 80°C overnight[18,19]. The whole process is shown in Fig. 1.

For comparison purposes, three additional samples, W-Mo(E) 0.95:0.05, W-Mo(E) 0.8:0.2, and W-Mo(E) 0.7:0.3 were synthesized under the same conditions in separate setups using the same volume of DES[18,19].

Photochromic activity of the nanocomposite

The powdered samples were placed on a clean sheet of white paper and pressed for the photochromic activity test. Light irradiation was performed on the sample for 24 s using a xenon lamp (B300 mW cm^2) UV-visible light source (Beijing NBET Technology

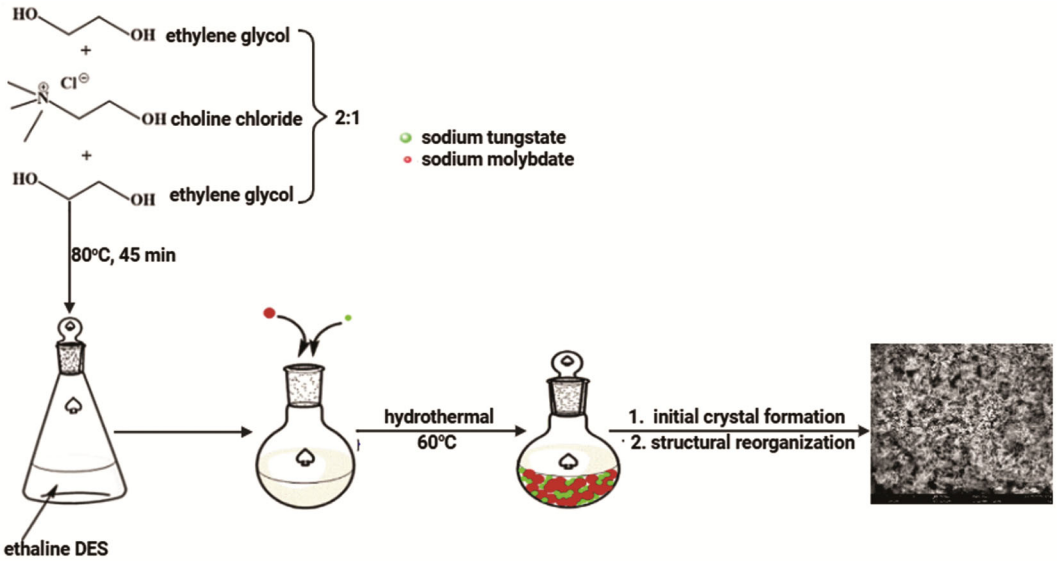

Fig. 1 — Schematic representation of the preparation method and resulting morphological changes in the nanocomposite

Co. Ltd). The reverse fading process was done in the open air at a room temperature[19].

Basic characterization of all the composites

Fourier-transform infrared (FTIR) spectroscopy was applied to identify the functional groups present in the synthesized composites. Data were collected using a Shimadzu 8400S spectrometer with KBr pellet samples, covering the 400-4000 cm^{-1} range at a resolution of 2.0 cm^{-1} to ensure sharp and well-defined absorption features. Structural phase analysis was performed by powder X-ray diffraction (PXRD) on a Rigaku Ultima IV diffractometer, operated with monochromatic Cu Kα radiation (λ = 0.15406 nm). Optical characteristics were assessed using a Shimadzu UV-2600 UV–visible spectrophotometer, recording both reflectance and transmittance spectra in the 200–800 nm wavelength range under ambient conditions. Morphological and microstructural observations were carried out with a scanning electron microscope (SEM, FEI model 110730002486) after sputter-coating the specimens with a thin conductive gold layer. The elemental composition of the materials was examined using an energy-dispersive X-ray (EDX) detector integrated into the SEM setup. SEM imaging was performed at an accelerating voltage of 45 kV with a beam current of 45 mA. Electrochemical impedance spectroscopy (EIS) measurements were conducted to investigate interfacial resistance and charge-transfer dynamics. The experiments were performed using a potentiostat/galvanostat system in the frequency range of 0.01 Hz to 100 kHz, applying a sinusoidal

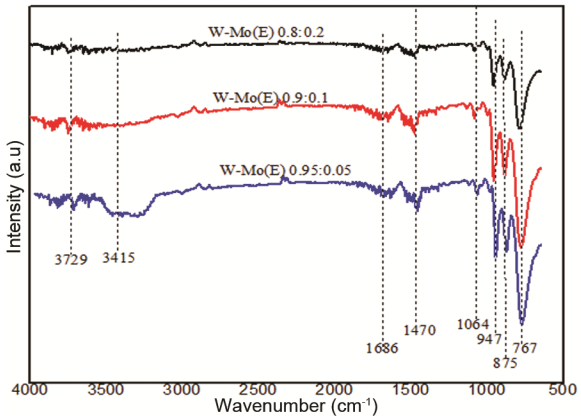

Fig. 2 — FTIR spectra of the resulting composites

perturbation of 10 mV at the open-circuit potential. The impedance data were represented as Nyquist plots and interpreted through equivalent circuit fitting to extract relevant electrochemical parameters.

Results and Discussion

FTIR analysis of the composites

The FTIR spectra of the composites, presented in Fig. 2, illustrate the presence of various functional groups through their characteristic absorption bands. While the functional groups appeared at similar wavenumbers across the samples, variations in peak intensity were observed. These differences are likely associated with interactions among the chemical species, particularly the enhancement of certain weak absorption bands originating from the deep eutectic solvent (DES) upon incorporation of metals at different ratios (0.9:0.1 and 0.8:0.2) to form the

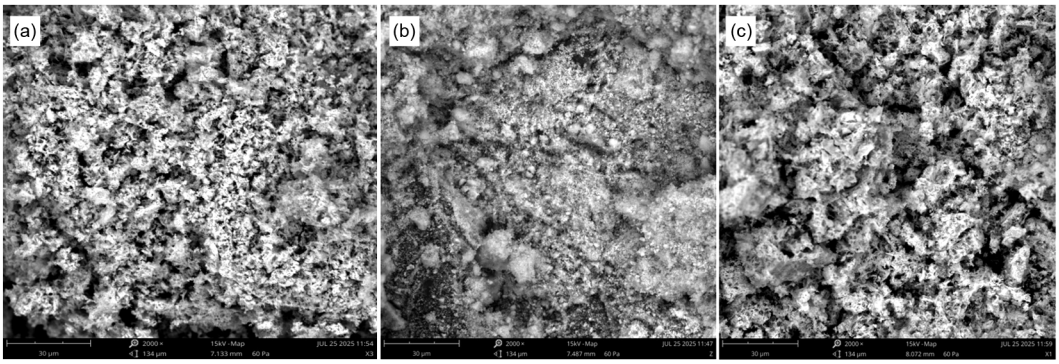

Fig. 3 — SEM images of the resulting composites: (a) W-Mo (E) 0.9:0.1, (b) W-Mo (E) 0.8:0.2 and (c) W-Mo (E) 0.7:0.3

Table 1 — Data summary from EDX showing the relative abundance of the element in the composites

Elements	W		C		O		Mo	
Composite/Composition (%)	W	A	W	A	W	A	W	A
W-Mo(E) 0.9:0.1	76.2	78.9	8.4	9.2	10.2	11.3	5.2	2.3
W-Mo(E) 0.8:0.2	67.3	70.2	11.2	13.9	13.4	10.3	8.1	5.6
W-Mo(E) 0.7:0.3	62.3	66.2	10.2	13.5	14.5	12.2	13.1	9.1

A: atomic percent; W: weight percent

W-Mo(E) 0.9:0.1 and W-Mo(E) 0.8:0.2 composites, respectively[20,21]. The spectra exhibited distinct vibrational features, including a sharp N-H stretching band at 3729 cm^{-1} and a broad O-H stretching band centered around 3415 cm^{-1}. Additionally, weaker bands at 1686 and 1470 cm^{-1} were identified, corresponding to C=O stretching and N-H bending vibrations typical of amide groups[22]. A modest peak at approximately 1064 cm^{-1} was attributed to C-O-C linkages. Moreover, absorption bands observed within the 947-767 cm^{-1} range were assigned to W-O and Mo-O stretching vibrations, indicative of tungsten-oxygen and molybdenum-oxygen bonding within the composite matrix[23,24].

SEM and Energy-Dispersive X-ray spectroscopy

The composites, produced at different mass ratios of transition metal oxides in a deep eutectic solvent medium, were examined by scanning electron microscopy (SEM). As shown in Fig. 3, the images reveal significant particle agglomeration, with compact clusters evident across the surface. Such aggregation is likely associated with structural reorganization during drying, where rapid solvent removal promotes interparticle contact. The particles exhibit predominantly irregular morphologies with coarse surface textures, and the size variation indicates heterogeneous nucleation and growth during synthesis[25]. Energy-dispersive X-ray spectroscopy (EDX) verified the presence of W, C, O, and Mo, with notable C and O abundances that are important for the reverse fading response of photochromic materials (Table 1)[25].

XRD analysis

X-ray diffraction analysis of the synthesized nanocomposites showed a distinct peak at 10.63° corresponding to (2 0 0) of ammonium tungsten oxide hydrate, $[5(NH_4)_2O{\cdot}12WO_3{\cdot}5H_2O]$ (JCPDS card No. 36-0101) is associated with the monoclinic structure of MoO_4, confirming its presence alongside WO_3. Other noticeable peaks at 6.92°, 13.31°, and 23.67° correspond to (-1 0 1), (-1 0 3), and (1 0 3) of the monoclinic tungsten oxide according to the standard pattern JCPDS card No 36-0101 (Fig. 4). The detection of this low-angle reflection indicates the simultaneous formation of hydrated and ammonium-containing tungsten oxide phases, alters the interlayer separation, and retains structural water within the lattice.

The diffraction features suggest a semi-crystalline nature, where aggregated particles consist of both ordered and disordered domains, as reflected by the mixture of well-defined and broadened peaks. A progressive reduction in peak intensity with increasing dopant loading implies that the dopant plays a crucial role in modifying the crystallization behavior of WO_3, possibly reducing crystallite dimensions and introducing structural defects[25]. In addition, the average particle size (D) was calculated using Scherrer's equation:

$$D = \frac{0.9\lambda}{\beta cos\theta} \quad \ldots (1)$$

Where λ is wavelength of Cu Kα radiation (λ =0.1518 nm), β is full width at half maximum of the diffraction plane, and θ is Bragg diffraction angle. Therefore, the average crystalline size from the intense peak was 20.47 nm.

EIS analysis

The Nyquist plots, as illustrated in Fig. 5, show semicircular arcs that are indicative of the interfacial charge transfer resistance (R_{ct}) between the nanocomposite and the electrolyte interface[31,32].

A comparative assessment between the W:Mo (0.9:0.1) and (0.8:0.2) samples reveals that the 0.8:0.2 nanocomposite exhibits a notably smaller semicircle. This corresponds to a lower R_{ct} value, suggesting enhanced electrical conductivity and more efficient charge carrier mobility across the electrode-electrolyte interface. The observed improvement can be attributed to the increased MoO_3 content, which contributes to a more interconnected structure, facilitating electron delocalization and accelerated charge transport[33,34].

This electrochemical behaviour plays a pivotal role in determining the material's photochromic response. The reduced charge transfer resistance observed in the 0.8:0.2 composite implies that photogenerated electrons can be more readily transferred through the material, thereby promoting faster and more reversible photochromic transitions[35,36].

Thus, the incorporation of an optimal molybdenum content not only enhances electrical conductivity but also supports improved photo-induced charge dynamics, which are essential for achieving high-performance photochromic materials.

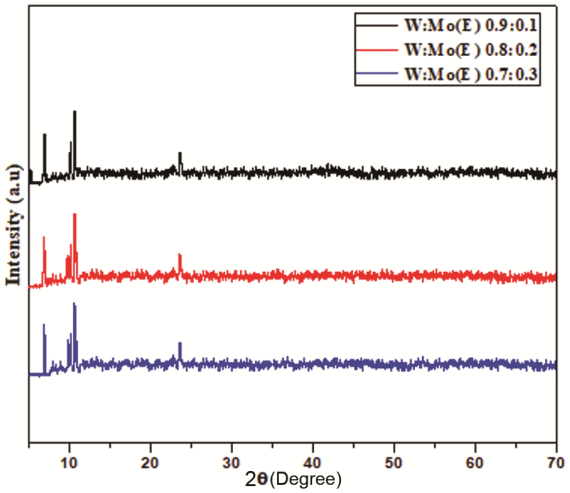

Fig. 4 —XRD plots of as-prepared samples at 80°C; W:Mo(E) 0.9:0.1; W:Mo(E)0.8:0.2; W:Mo(E) 0.7:0.3

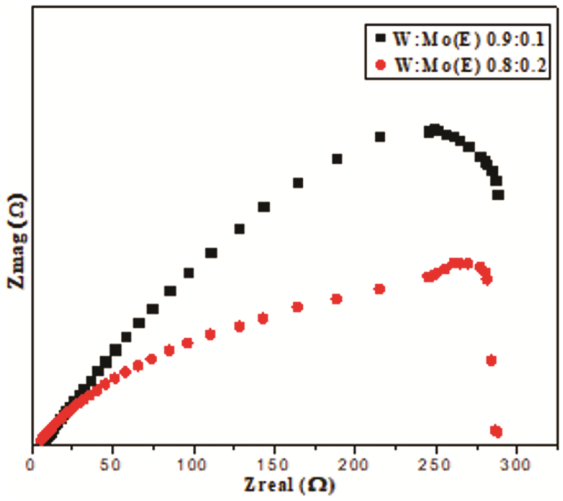

Fig. 5 — EIS spectra of as-prepared samples at 80°C; W:Mo(E) 0.9:0.1 and W:Mo(E) 0.8:0.2

UV-visible spectroscopy analysis

The photochromic response of transition metal oxide nanocomposites is known to be highly dependent on both the dopant concentration and the synthesis medium. Varying mass ratios of molybdenum (0.05, 0.1, 0.2, and 0.3g of Mo) were incorporated into a WO_3 matrix to evaluate their effect on optical properties and colour-switching efficiency. The absorption spectra (Fig. 6) confirmed that increasing Mo content enhanced light absorption across the UV-visible region. This behaviour aligns with previous reports where

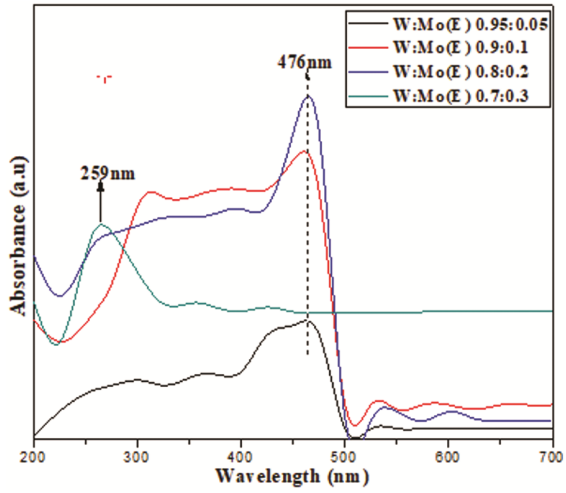

Fig. 6 — UV-visible screening of the photochromic responses of different nanocomposites before exposure to UV-light

transition metal dopants, such as Cu^{2+}, introduced additional donor states that effectively narrowed the bandgap of WO_3, thus extending the photo response into the visible light region[29].

UV-visible screening of the photochromic responses of the nanocomposite after exposure to light at different time intervals is shown in Fig. 7. The optimal photochromic behaviour was observed at a Mo loading of 0.2 g, where a pronounced colouration, bleaching reversibility, and increased light absorption were recorded. This enhanced performance is due to improved charge separation and suppressed electron-hole recombination, facilitated by the substitution of W^{6+} with Mo^{6+} ions[29] (Fig. 8). Similar trends have been reported in Cu-doped WO_3 systems, where moderate doping levels improve photoactivity, while excessive dopant concentrations result in defect states that act as recombination centers, reducing overall

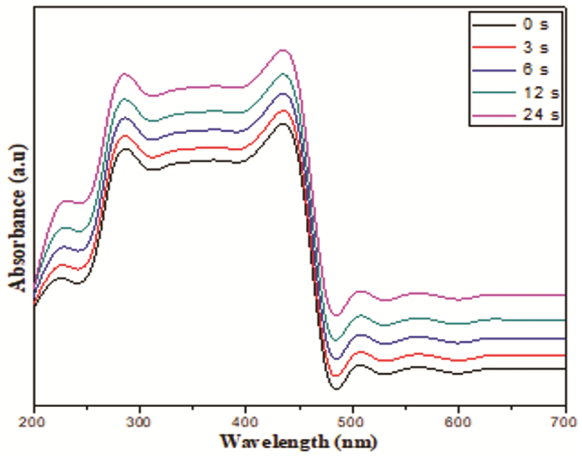

Fig. 7 — UV-visible screening of the photochromic responses of the nanocomposite after exposure to light at different time intervals

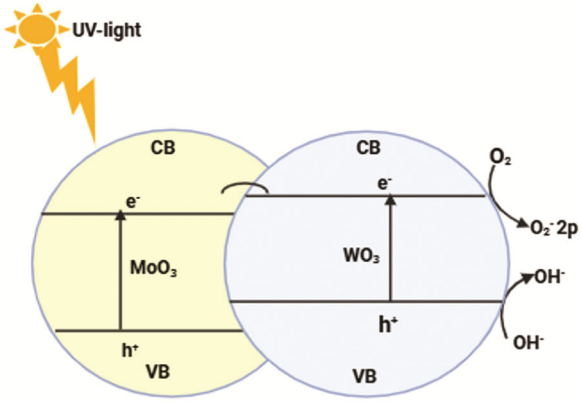

Fig. 8 — Schematic illustration of the excitation and electron transfer in the photochromic binary metal oxide nanocomposites

efficiency[29]. The 0.05 g Mo sample displayed weak optical absorption, suggesting insufficient dopant levels for meaningful alteration of the electronic structure.

In contrast, the 0.3 g Mo sample exhibited diminished visible light activity, with absorption restricted largely to the UV region, due to oversaturation of Mo leading to structural disorder or the formation of non-conductive molybdate phases[19].

Furthermore, the role of deep eutectic solvents (DES) as the reaction medium was critical in tailoring the morphological and optical characteristics of the composites. The DES used comprises quaternary ammonium salts (choline chloride) and hydrogen bond donors (ethylene glycol) molecules, promoting the formation of uniform nanostructures and a hydrogen-bonded network conducive to electron mobility. Prior studies have shown that DESs influence nucleation, particle growth, and surface properties of metal oxides, affecting charge transport and redox behavior[8,10]. In particular, DESs' alcohol-based hydrogen bond donors contribute protons essential for the photo-induced redox reactions, thus facilitating the reversible colour change.

Additionally, the presence of the quaternary ammonium group (R_3N^+) within the DES matrix further assists in photogenerated electron transfer processes. These cationic centers are known to promote charge separation at the oxide interface; an effect observed in DES-mediated synthesis of photochromic materials such as V_2O_5 and TiO_2[10,11]. The hydrogen bonding interactions between chloride anions and ethylene glycol further stabilize the reaction environment, enabling uniform dispersion of the molybdenum oxide and contributing to the consistent optical behaviour across the composite samples [12,13].

Taken together, the findings indicate that both the MoO_3 and the DES-assisted synthesis route are critical parameters in tuning the photochromic performance of W-Mo (E) nanocomposites. The observed enhancement in colouration reversibility and absorption characteristics for the 2 g Mo sample underscores the importance of optimizing dopant concentration to balance electronic structure modification with structural integrity. These results provide insight into the design of advanced photochromic materials using transition metal oxides and sustainable solvent systems for smart optoelectronic applications.

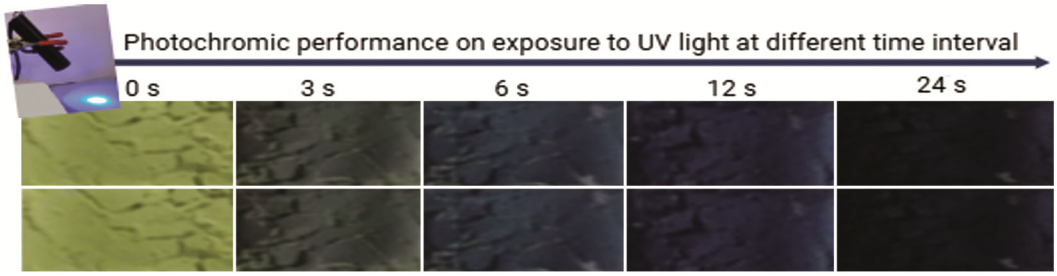

Fig. 9 — Visible eye screening before and after the exposure to UV-light

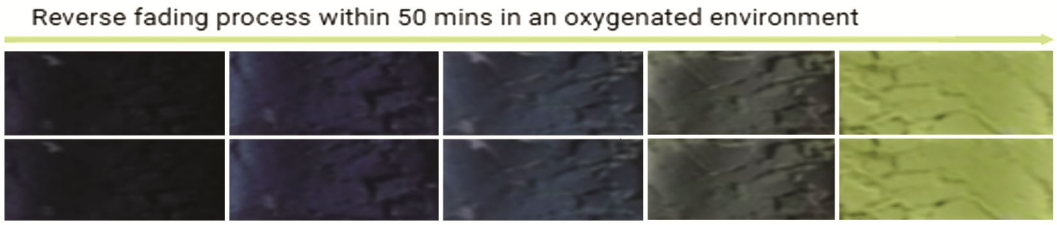

Fig. 10 — Reverse fading process at different time intervals

Photochromism behaviour of the composites

The photochromic response of the as-prepared W-Mo(E) was investigated under visible light irradiation using a 300 mW cm^{-2} xenon lamp. As shown in Fig. 9, the composite initially displayed a creamy yellow colour, which transformed into a distinct blue hue within three seconds of exposure. The colouration intensity increased with prolonged irradiation, reaching saturation after approximately 24 s. This rapid, light-induced transition and its reversibility suggest a highly active photochromic mechanism operating within the W-Mo oxide matrix[29].

The observed optical transformation is characteristic of transition metal oxides with mixed-valence states. In particular, both W and Mo are known for their ability to undergo reversible redox reactions under photon excitation. Upon exposure to visible light, electron transfer is initiated within the lattice, leading to the reduction of W^{6+} to W^{5+} and Mo^{6+} to Mo^{5+}. These reduced species introduce localized electronic states in the bandgap, contributing to visible light absorption and thus the appearance of blue coloration[9,13]. This mechanism is consistent with earlier studies on WO_3 and MoO_3 films, where photochromic switching was attributed to intervalence charge transfer (IVCT) between adjacent W or Mo cations in different oxidation states[13].

In this W-Mo system, the interplay between both metal centers further enhances the electron hopping process. The intervalence charge transfer can occur not only between similar ions (W^{6+}/W^{5+} or Mo^{6+}/Mo^{5+}) but also across different metal centers ($Mo^{5+} \rightarrow W^{6+}$ or $W^{6+} \rightarrow Mo^{5+}$), facilitating a dynamic and efficient redox process[9,10]. The mixed oxide matrix, enriched with multiple valence states (W^{6+}, W^{5+}, Mo^{6+}, Mo^{5+}), creates a conducive environment for fast coloration under light and stable bleaching in the dark[16,18].

The reversibility of this process was demonstrated by allowing the irradiated sample to recover in a dark, oxygen-rich environment (Fig. 10). Within 50 min, the blue coloration faded, and the sample returned to its original creamy yellow color. This behavior is indicative of the reoxidation of W^{5+} and Mo^{5+} back to their respective +6 oxidation states, a process commonly reported in reversible photochromic systems[13]. Oxygen in the atmosphere acts as an electron scavenger, facilitating the restoration of the initial valence state and thereby enabling the bleaching mechanism[19].

The significant decrease in reflectance intensity in the visible region during light exposure further confirms the formation of photo-induced absorption bands. These bands are attributed to the transition of electrons from oxygen 2p orbitals to the d orbitals of W and Mo atoms, or to the creation of polaronic states that absorb visible light[8,9]. Notably, the coloration intensity saturated after 24 s, suggesting the redox process reached a thermodynamic limit under continuous illumination (Fig. 9).

The synthesis route using DES may also contribute to the photochromic enhancement. The DES environment introduces protons and facilitates uniform dispersion of metal ions, which enhances the

structural homogeneity and the mobility of charge carriers[29]. Studies have shown that DES-based synthesis often results in smaller particle sizes and a high concentration of surface-active sites, both of which are beneficial for fast redox kinetics and strong coloration effects in metal oxides[29,30].

Conclusion

Tungsten oxide-molybdenum oxide (WO_3-MoO_3) nanocomposites were successfully synthesized via Ethaline. Characterization confirmed the effective incorporation of metal oxides into the DES matrix, with FTIR revealing characteristic metal-oxygen interactions and SEM showing irregular, agglomerated particle morphologies. XRD analysis indicated the formation of a monoclinic semicrystalline phase. The nanocomposites exhibited a rapid and reversible photochromic response, transitioning from pale yellow to deep blue under UV irradiation, supported by UV-visible spectral changes involving LMCT and d-d transitions. Electrochemical impedance spectroscopy further validated the enhanced charge transport and interfacial conductivity of the DES-assisted composites, confirming efficient electron mobility critical to their photochromic switching behaviour. The stable and responsive performance under anaerobic conditions highlights the potential of these materials for advanced applications in smart windows, optical switches, and photo-responsive coatings.

Conflict of interest

The authors declare no conflict of interest.

References

1 Zhou Y, Zhi M & Wei B, Recent advances in tungsten oxide-based photochromic and electrochromic materials, *J Mater Chem C*, 10 (2022) 4607.

2 Kayani A B A, Kuriakose S, Monshipouri M, Khalid F A, Walia S, Sriram S & Bhaskaran M, UV photochromism in transition metal oxides and hybrid materials, *Small*, 17 (2021) 2100621.

3 Zhang C R, Cui W R, Niu C P, Yi S M, Liang R P, Qi J X, Chen X J, Jiang W, Zhang L & Qiu J D, rGO-based covalent organic framework hydrogel for synergistically enhancing uranium capture capacity through photothermal desalination, *Chem Eng J*, 428 (2022) 131178.

4 Liu L, Shi J, Sun X, Zhang Y, Qin J, Peng S, Xu J, Song L & Zhang Y, Thermoresponsive hydrogel-supported antibacterial material with persistent photocatalytic activity for continuous sterilization and wound healing, *Compos Part B: Eng*, 229 (2022) 109459.

5 Zhao H, Cun Y, Bai X, Xiao D, Qiu J, Song Z, Liao J & Yang Z, Entirely reversible photochromic glass with high coloration and luminescence contrast for 3D optical storage, *ACS Energy Lett*, 7 (2022) 2060.

6 Bardestani R, Patience G S & Kaliaguine S, Experimental methods in chemical engineering: Specific surface area and pore size distribution measurements, BET, BJH, and DFT, *Canad J Chem Eng*, 97 (2019) 2781.

7 Sharma A K, Pandey S, Sharma K H, Nerthigan Y, Khan M S, Hang D R & Wu H F, Two-dimensional α-MoO_{3-x} nanoflakes as a bare eye probe for hydrogen peroxide in biological fluids, *Anal Chim Acta*, 1015 (2018) 58.

8 Ye S, Ma W, Shao W, Ejeromedoghene O, Fu G & Kang M, Gradient dynamic cross-linked photochromic multifunctional polyelectrolyte hydrogels for visual display and information storage application, *Polymer*, 243 (2022) 124642.

9 Ejeromedoghene O, Ma X, Oderinde O, Yao F, Adewuyi S & Fu G, Quaternary type IV deep eutectic solvent-based tungsten oxide/niobium oxide photochromic and reverse fading composite complex, *New J Chem*, 45 (2021) 18008.

10 Kumar S G & Rao K S R K, Tungsten-based nanomaterials (WO_3 & Bi_2WO_6): modifications related to charge carrier transfer mechanisms and photocatalytic applications, *Appl Surf Sci*, 355 (2015) 939.

11 Zhang A, Liang Y, Zhang H, Geng Z & Zeng J, Doping regulation in transition metal compounds for electrocatalysis, *Chem Soc Rev*, 50 (2021) 9817.

12 Mou H, Wang J, Zhang D, Yu D, Chen W, Wang D & Mu T, A one-step deep eutectic solvent-assisted synthesis of carbon nitride/metal oxide composites for photocatalytic nitrogen fixation, *J Mater Chem A*, 7 (2019) 5719.

13 Oderinde O, Hussain I, Kang M, Wu Y, Mulenga K, Adebayo I, Yao F & Fu G, Water as DES cosolvent on the morphology tuning and photochromic enhancement of tungsten oxide-molybdenum oxide nanocomposite, *J Ind Eng Chem*, 80 (2019) 1.

14 Sun N, Ji R, Zhang F, Song X, Xie A, Liu J, Zhang M, Niu L & Zhang S, Structural evolution in poly(acrylic-co-acrylamide) pH-responsive hydrogels by low-field NMR, *Mater Today Commun*, 22 (2020) 100748.

15 Wei J, Jiao X, Wang T & Chen D, The fast and reversible intrinsic photochromic response of hydrated tungsten oxide nanosheets, *J Mater Chem C*, 3 (2015) 7597.

16 Yao Y, Sang D, Zou L, Wang Q & Liu C, A review on the properties and applications of WO_3 nanostructure-based optical and electronic devices, *Nanomaterials*, 11 (2021) 2136.

17 Andron I, Marichez L, Jubera V, Labrugère C, Duttine M, Frayret C & Gaudon M, Photochromic behavior of ZnO/MoO_3 interfaces, *ACS Appl Mater Interf*, 12 (2020) 46972.

18 Oderinde O, Ejeromedoghene O & Fu G, Synthesis and properties of low-cost, photochromic transparent hydrogel based on ethaline-assisted binary tungsten oxide-molybdenum oxide nanocomposite for optical memory applications, *Polym Adv Technol*, 33 (2022) 687.

19 Ejeromedoghene O, Oderinde O, Yao F, Adewuyi S & Fu G, Intrinsic structural/morphological and photochromic responses of WO_3 co-doped MoO_3 nanocomposites based on varied drying methods, *Dry Technol*, 21 (2021) 1.

20 Ru Y, Shi Z, Zhang J, Wang J, Chen B, Huang R, Liu G & Yu T, Recent progress of photochromic materials towards photocontrollable devices, *Mater Chem Front*, 5 (2021) 7737.

21 Farid-Ul-Haq M, Hussain M A, Haseeb M T, Ashraf M U, Hussain S Z, Tabassum T, Hussain I, Sher M, Bukhari S N A & Naeem-Ul-Hassan M, A stimuli-responsive, superporous and non-toxic smart hydrogel from seeds of mugwort (Artemisia vulgaris): stimuli responsive swelling/deswelling, intelligent drug delivery and enhanced aceclofenac bioavailability, *RSC Adv*, 10 (2020) 19832.

22 Tomé L C & Mecerreyes D, Emerging ionic soft materials based on deep eutectic solvents, *J Phys Chem B*, 124 (2020) 8465.

23 Vernickaite E, Lelis M, Tsyntsaru N, Pakštas V & Cesiulis H, XPS studies on the Mo oxide-based coatings electrodeposited from highly saturated acetate bath, *Chemija*, 3 (2020) 203.

24 Xu H, Zhang L, Wang A, Hou J & Guo X, Facile preparation of oxygen-vacancy-engineered MoO_x nanostructures for photoreversible switching systems, *Nanomaterials*, 11 (2021) 3192.

25 Hasani A, Van-Le Q, Nguyen T P, Choi K S, Sohn W, Kim J K K, Jang H W & Kim S Y, Facile solution synthesis of tungsten trioxide doped with nanocrystalline molybdenum trioxide for electrochromic devices, *Sci Rep*, 7 (2017) 13258.

26 Ge X, Gu C, Wang X & Tu J, Deep eutectic solvents (DESs)-derived advanced functional materials for energy and environmental applications: Challenges, opportunities, and future vision, *J Mater Chem A*, 5 (2017) 8209.

27 Pandey A & Pandey S, Solvatochromic probe behavior within choline chloride-based deep eutectic solvents: effect of temperature and water, *J Phys Chem B*, 118 (2014) 14652.

28 Song Y, Zhao J, Zhao Y & Huang Z, Aqueous synthesis and photochromic study of Mo/WO oxide hollow microspheres, *RSC Adv*, 6 (2016) 99898.

29 Bingbing C, Chuanpan G, Guodong F & Zhihong Z, Photochromic performance of hydrogel based on deep eutectic solvent induced water-soluble Cu-doped WO_3 hybrids with antibacterial property, *J Photochemi Photobiol, A: Chem*, 435 (2023) 114320.

30 Oderinde O, Kang M, Kalulu M, Yao F & Fu G, Facile synthesis and study of the photochromic properties of deep eutectic solvent-templated cuboctahedral-WO_3/MoO_3 nanocomposites, *Superlattices Microstruct*, 125 (2019) 103.

31 Jittiarporn P, Sikong L, Kooptarnond K, Taweepreda W, Stoenescu S, Badilescu S & Truong V V, Electrochromic properties of MoO_3-WO_3 thin films prepared by a sol-gel method in the presence of a triblock copolymer template, *Surf Coat Technol*, 327 (2017) 66.

32 El-Hajjaji F, Aouniti A, Al-Deyab A, Chetouani A, Hammouti B & Radi S, Electrochemical impedance spectroscopy (EIS) for corrosion evaluation of metal alloys, *J Mol Liq*, 275 (2019) 879.

33 Olasunkanmi L O & Ebenso E E, Nanostructured corrosion inhibitors: A review of electrochemical mechanisms, *J Mol Struct*, 1203 (2020) 127418.

34 Kiani A, Rahimi E & Abdollahi M, Improved charge transfer and photocatalytic activity of MoO_3-WO_3 nanocomposites, *Ceram Int*, 47 (2021) 24344.

35 Bahloul A, Hmida I, Guesmi F & Ammar S, Deep eutectic solvent-assisted synthesis of metal oxide nanostructures: Influence on electrochemical and optical performance, *Electrochim Acta*, 445 (2023) 141765.

36 Wu L, Ye X, Zhou L, Jiang Y & Chen Y, High-performance WO_3-based photochromic devices with enhanced switching dynamics, *ACS Appl Mater Interf*, 10 (2018) 5552.